

LETTER TO THE EDITOR

Determining dust temperatures and masses in the *Herschel* era: the importance of observations longward of 200 micron[★]

K. D. Gordon¹, F. Galliano², S. Hony², J.-P. Bernard³, A. Bolatto⁴, C. Bot⁵, C. Engelbracht⁶, A. Hughes^{7,8}, F. P. Israel⁹, F. Kemper¹⁰, S. Kim¹¹, A. Li¹², S. C. Madden², M. Matsuura^{13,14}, M. Meixner^{1,15}, K. Misselt⁶, K. Okumura², P. Panuzzo², M. Rubio¹⁶, W. T. Reach^{17,18}, J. Roman-Duval¹, M. Sauvage², R. Skibba⁶, and A.G.G.M. Tielens⁹

(Affiliations can be found after the references)

Preprint online version: October 30, 2018

ABSTRACT

Context. The properties of the dust grains (e.g., temperature and mass) can be derived from fitting far-IR SEDs ($\geq 100 \mu\text{m}$). Only with SPIRE on *Herschel* has it been possible to get high spatial resolution at 200 to 500 μm that is beyond the peak ($\sim 160 \mu\text{m}$) of dust emission in most galaxies. **Aims.** We investigate the differences in the fitted dust temperatures and masses determined using only $< 200 \mu\text{m}$ data and then also including $> 200 \mu\text{m}$ data (new SPIRE observations) to determine how important having $> 200 \mu\text{m}$ data is for deriving these dust properties.

Methods. We fit the 100 to 350 μm observations of the Large Magellanic Cloud (LMC) point-by-point with a model that consists of a single temperature and fixed emissivity law. The data used are existing observations at 100 and 160 μm (from IRAS and *Spitzer*) and new SPIRE observations of 1/4 of the LMC observed for the HERITAGE Key Project as part of the *Herschel* Science Demonstration phase.

Results. The dust temperatures and masses computed using only 100 and 160 μm data can differ by up to 10% and 36%, respectively, from those that also include the SPIRE 250 & 350 μm data. We find that an emissivity law proportional to $\lambda^{-1.5}$ minimizes the 100–350 μm fractional residuals. We find that the emission at 500 μm is $\sim 10\%$ higher than expected from extrapolating the fits made at shorter wavelengths. We find the fractional 500 μm excess is weakly anti-correlated with MIPS 24 μm flux and the total gas surface density. This argues against a flux calibration error as the origin of the 500 μm excess. Our results do not allow us to distinguish between a systematic variation in the wavelength dependent emissivity law or a population of very cold dust only detectable at $\lambda \geq 500 \mu\text{m}$ for the origin of the 500 μm excess.

Key words. ISM: general – Galaxies: individual: LMC – Magellanic Clouds – Infrared: ISM

1. Introduction

Among nearby galaxies, the Large Magellanic Cloud (LMC) and Small Magellanic Cloud (SMC) represent unique astrophysical laboratories for interstellar medium (ISM) studies. Both Clouds are relatively nearby, the LMC at ~ 50 kpc (Schaefer 2008) and the SMC at ~ 60 kpc (Hilditch et al. 2005), and provide ISM measurements that are relatively unconfused by line-of-sight uncertainties when compared to the Milky Way. The two Clouds span an interesting metallicity range with the LMC at $\sim 1/2 Z_{\odot}$ (Russell & Dopita 1992) being above the threshold of $1/3$ – $1/4 Z_{\odot}$ where the properties of the ISM change as traced by the rapid reduction in the PAH dust mass fractions and possible dust-to-gas ratios (Draine et al. 2007) and the SMC at $\sim 1/5 Z_{\odot}$ (Russell & Dopita 1992) below this threshold. Finally, the dust in the LMC and SMC shows strong variations in its ultraviolet characteristics (Gordon et al. 2003).

The HERschel Inventory of The Agents of Galaxy Evolution (HERITAGE) in the Magellanic Clouds *Herschel* Key Project will map both Clouds using the PACS/SPIRE Parallel observing mode providing observations at 100, 160, 250, 350, and 500 μm (Meixner, M. et. al. 2010). The HERITAGE wavelength coverage (100–500 μm) and spatial resolution (~ 10 pc at 500 μm) is well suited to measuring the spatial variations of dust temperatures and masses. The infrared dust emission in most galaxies

peaks between 100–200 μm (Dale et al. 2005) and observations $> 200 \mu\text{m}$ are important for accurate dust temperature and masses (Willmer et al. 2009). Ground-based submillimeter observations do provide the needed $> 200 \mu\text{m}$ observations, but they have been seen to be in excess of that expected from extrapolating fits to the $< 200 \mu\text{m}$ data for sub-solar metallicity galaxies (Galliano et al. 2005). This excess could be due to very cold dust that only emits at submillimeter wavelengths or variations in the wavelength dependent dust emissivity law (Reach et al. 1995; Paradis et al. 2009a). As part of the Science Demonstration Program (SDP), two HERITAGE AORs centered on the LMC were executed. These observations are used in this paper to explore the impact SPIRE observations have on the measurement of dust temperatures and masses including the behavior of any submillimeter excess.

2. Data

The observation and data reduction for the HERITAGE SDP data are given in Meixner, M. et. al. (2010). For this paper, we use high quality IRAS 100 μm and MIPS 160 μm observations instead of the PACS observations which display large residual instrumental signatures (expected to be eliminated with the full HERITAGE dataset). We extracted the HERITAGE SDP region from the existing IRAS/IRIS 100 μm (Miville-Deschênes & Lagache 2005) and MIPS 160 μm (Meixner et al. 2006; Bernard et al. 2008) mosaics. We have used custom convolution kernels created using the technique of

[★] *Herschel* is an ESA space observatory with science instruments provided by European-led Principal Investigator consortia and with important participation from NASA.

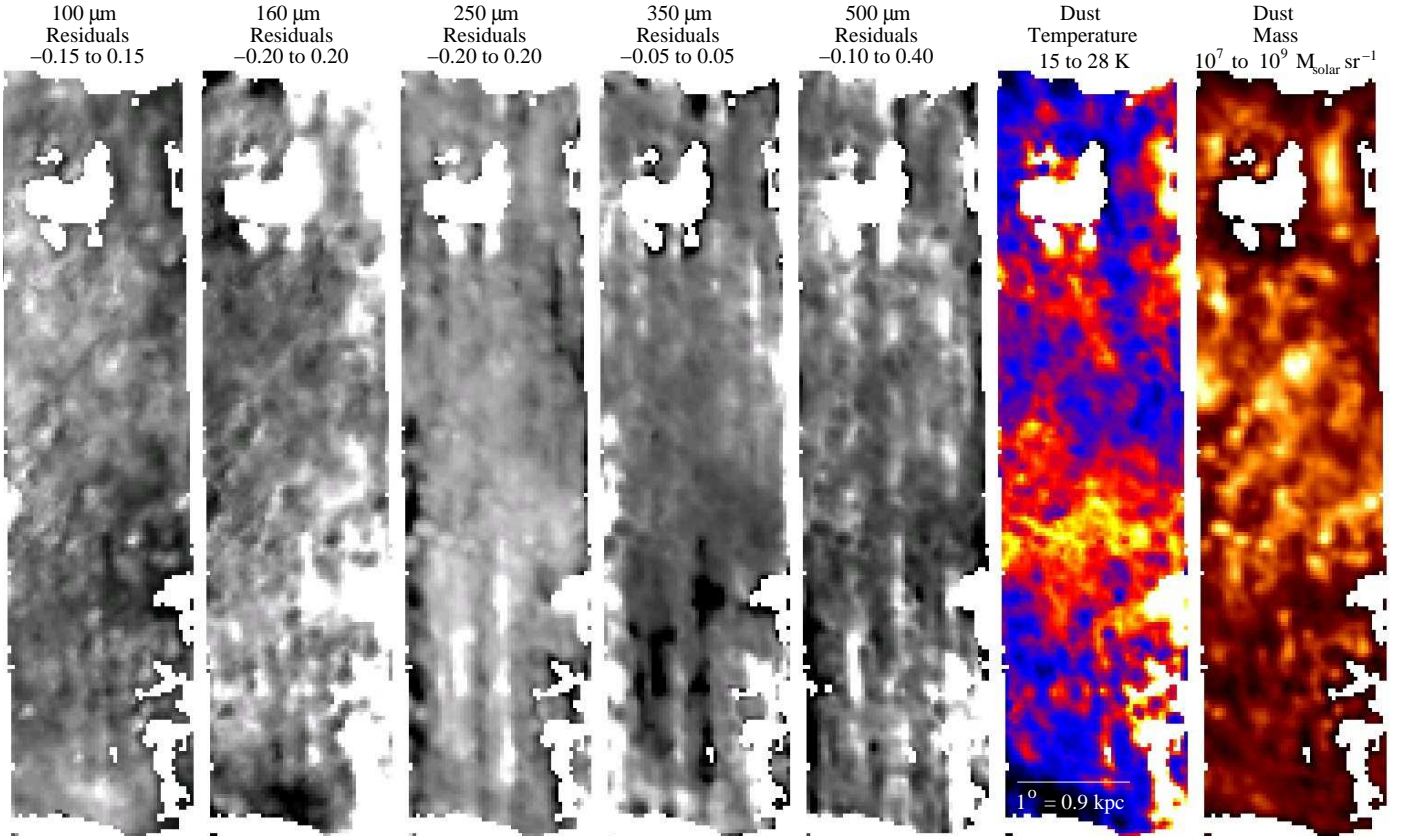


Fig. 1. The best fit (assuming an emissivity law with $\beta = 1.5$) dust temperature and mass images are shown along with the fractional residual images at all 5 bands. The resolution of all the images is $4'.3$. Each of the fractional residual images shows the difference in flux between the measured value and best fit model divided by the best fit model. They are separately linearly scaled (black to white) to emphasize the structure and the scale ranges are given at the top of each of the images. The dust temperature image is linearly scaled between 18 (blue) and 28 K (yellow). The dust mass image has a sqrt scaling between 10^7 (black) and 10^9 (yellow) M_{\odot}/sr . The vertical white and black streaks in the SPIRE fractional residual images are caused by residual instrumental signatures.

Gordon et al. (2008) to convolve the images to a common resolution of $4'.3$ of the IRAS $100 \mu\text{m}$ data. We also created a 2nd set of images (excluding the IRAS $100 \mu\text{m}$ data) at the common resolution of the SPIRE $500 \mu\text{m}$ and MIPS $160 \mu\text{m}$ data of $\sim 38''$.

Emission from Milky Way (MW) foreground cirrus clouds contributes to the far-IR emission seen in the LMC. We use the HI column density map created by integrating the MW velocities in the full HI cube (Staveley-Smith et al. 2003) to correct all the images for the MW infrared cirrus emission. The HI column densities were transformed to IR surface brightnesses using the model of the MW emission used by Bernard et al. (2008). Finally, any residual emission was removed by fitting a gradient across the SDP region using the regions in the strip beyond the IR edge of the LMC.

3. Results

For each point in the image, we determined the dust temperature by fitting the observed far-IR SED to a modified black body of the form

$$F_{\nu} \propto \lambda^{-\beta} B_{\nu}(T_{\text{dust}}) \quad (1)$$

The dust mass is computed from the measured $160 \mu\text{m}$ flux (F_{160}), at each point, using

$$M_{\text{dust}} = \frac{4}{3} \frac{a \rho d^2}{Q_{\text{em}}(160) B_{\nu}(T_{\text{dust}})} F_{160} \quad (2)$$

where $a = 0.1 \mu\text{m}$ is the grain radius, the grains are assumed to be spherical silicate grains with a density $\rho = 3 \text{ g cm}^{-3}$, $d = 50 \text{ kpc}$ is the LMC distance, and $Q_{\text{em}}(160) = 5.5 \times 10^{-4}$ (Laor & Draine 1993). This method is fairly standard and while other more sophisticated fitting methods exist (Draine et al. 2007; Galliano et al. 2008; Paradis et al. 2009b), this simple model allows us to probe the effects of adding $>200 \mu\text{m}$ data to the fits with fewest assumptions. We restrict our fits to using only data $\geq 100 \mu\text{m}$ as observations at shorter wavelengths likely include non-equilibrium dust grain emission (transient heating). The data points used in the fits were weighted by the uncertainties (i.e., $1/\sigma^2$). The main uncertainties on the measurements are the calibration and background noise uncertainties and we sum them in quadrature. The calibration errors are assumed to be approximately the same at all bands at around 15% (Stansberry et al. 2007; Swinyard, B. et. al. 2010). Data within 1σ of the background are not used in the fits.

3.1. Dust temperatures and masses

The best fit dust temperature and mass values were determined by fits using only the pre-*Herschel* data (IRAS $100 \mu\text{m}$ and MIPS $160 \mu\text{m}$) and fits including the *Herschel* SPIRE data (IRAS $100 \mu\text{m}$, MIPS $160 \mu\text{m}$, and SPIRE $250/350 \mu\text{m}$). Given the inclusion of the IRAS $100 \mu\text{m}$, we used the $4'.3$ resolution images. The SPIRE $500 \mu\text{m}$ data are not included in these fits as it is usually systematically high (see Sec. 3.2 and Meixner, M. et. al.

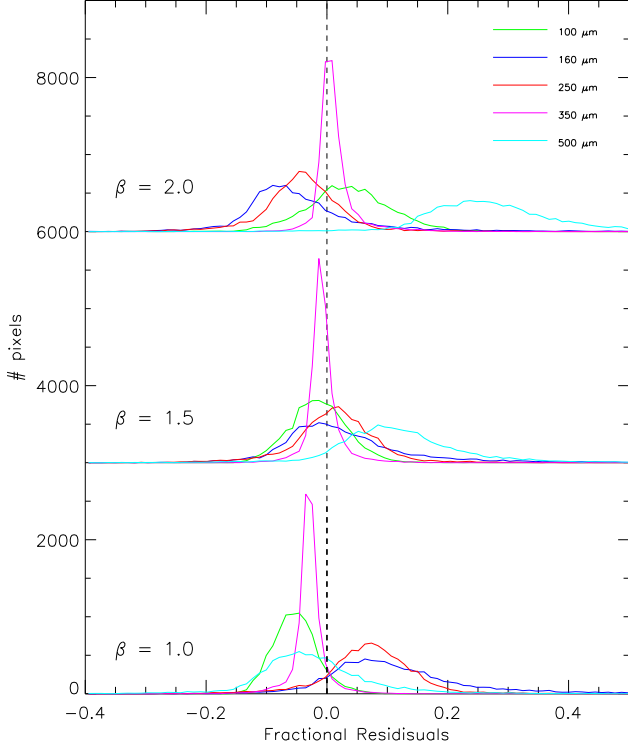


Fig. 2. The histograms of the fractional residuals at different wavelengths are shown for $\beta = 1.0, 1.5,$ and 2.0 . The fractional residual is the difference in flux at each wavelength between the measured and best fit model divided by the best fit model. The $\beta = 1.5$ and 2.0 histograms are offset by 3000 and 6000 pixels, respectively. The dashed vertical line indicates zero fractional residual. The strongly peaked $350 \mu\text{m}$ histogram is simply a result of the relative weighting of different wavelengths in the fit. For example, using equal weights produces more equally peaked histograms between the different wavelengths.

(2010)) and including it in the fits only causes the residuals at the other wavelengths to increase without significantly improving the fit. The value of β used in the fits was set to 1, 1.5, or 2 as this range encompasses realistic dust grains (amorphous to crystalline grains) and is what has been used in the past (Dunne et al. 2000). The dust temperature and mass maps and fractional residual images for the $\beta = 1.5$ case are shown in Fig. 1.

The differences between the best fit dust temperatures and masses (with and without the SPIRE data) depends on the value of β used. For $\beta = 2$, the with SPIRE to without SPIRE temperature ratio is 0.97 ± 0.06 and mass ratio is 1.19 ± 0.31 . For $\beta = 1.5$, the with/without SPIRE temperature ratio is 1.02 ± 0.07 and mass ratio is 0.96 ± 0.25 . For $\beta = 1$, the with/without temperature ratio is 1.08 ± 0.08 and mass ratio is 0.77 ± 0.20 . Thus, the inclusion of $> 200 \mu\text{m}$ data in the fits can change the derived dust temperature by up to 8% and mass by up to 23% depending on the assumed value of β .

Prior to the *Herschel* observations, it was not possible to constrain the best value of β given that there were only two infrared maps of the LMC with $\lambda \geq 100 \mu\text{m}$. With the *Herschel* observations, the behavior of the residuals as a function of β can be used to determine the optimal β value. Histograms of the fractional residuals at different β values are shown in Fig. 2. A value

of $\beta = 1.5$ clearly minimizes the fractional residuals at all wavelengths with most of the pixels having residuals of less than 10% at all wavelengths except $500 \mu\text{m}$. This result implies that either the characteristics of the dust grains are intermediate between the two extremes or that a more complex dust emission model including a distribution of dust temperatures and grain sizes is needed (Draine et al. 2007; Paradis et al. 2009b). Assuming a $\beta = 2.0$ for the pre-*Herschel* fits (a common assumption) and using the best fit $\beta = 1.5$ for the fits including the SPIRE data, we find the with/without temperature ratio is 1.12 ± 0.07 and mass ratio is 0.64 ± 0.16 . This decrease in dust masses reduces the magnitude of the “FIR excess” found by Bernard et al. (2008) for the LMC. Roman-Duval, J. et. al. (2010) explore this issue in detail for two specific LMC molecular clouds.

3.2. $500 \mu\text{m}$ excess

In the previous section, we have not included the $500 \mu\text{m}$ observations in the analysis as it was seen not to improve the quality of the fits and previous studies (Galliano et al. 2005; Galametz et al. 2009) have observed submm fluxes in excess of that expected from fits to the far-IR fluxes. At $4'3$ resolution, the average fractional $500 \mu\text{m}$ fit residual is 0.25, 0.10, and -0.05 for β values of 2, 1.5, and 1 (Fig. 2). As $\beta = 1.5$ is strongly favored as it minimizes the residuals at all other wavelengths, we find a $500 \mu\text{m}$ excess of approximately 10%. We find the same level of $500 \mu\text{m}$ excess for fits done at both the $4'3$ and $38''$ resolutions.

There are four possible origins of the $500 \mu\text{m}$ excess: 1) systematics due to our assumptions on our fitting, 2) a flux calibration error, 3) variations in the wavelength dependent emissivity law (Reach et al. 1995; Agladze et al. 1996), and 4) very cold dust that mostly emits at $\geq 500 \mu\text{m}$ (Finkbeiner et al. 1999; Galliano et al. 2005). Whatever the physical process responsible for the $500 \mu\text{m}$ excess, the HERITAGE SDP SPIRE data of the LMC allow us to probe the origin of the $500 \mu\text{m}$ excess at high spatial resolution in an external galaxy for the first time. We tested the systematics of our fitting algorithm and searched for correlations of the $500 \mu\text{m}$ excess with different tracers of the ISM conditions (dust temperature, dust mass, HI mass, and MIPS $24 \mu\text{m}$ flux) in an attempt to determine the origin of the $500 \mu\text{m}$ excess. The two strongest correlations are seen for MIPS $24 \mu\text{m}$ flux (probing the ISM conditions for small grains) and the total gas mass (probing the ISM density) are shown in Fig. 3.

To test 1), we performed Monte Carlo simulations where the observations were simulated both with and without an excess at $500 \mu\text{m}$ and with different β values. These simulations were fit with varying β laws and realistic uncertainties. A $500 \mu\text{m}$ excess was found in the simulations if it was part of the simulation or if the fitting β was smaller than the simulation β . Given that we empirically determine β from the $< 500 \mu\text{m}$ data, our conclusion is that the excess we find is not a result of our fitting method.

For 2), it is possible that there is a systematic $500 \mu\text{m}$ flux calibration error on the order of 10%. The official maximal possible flux calibration error for SPIRE is 15% at any wavelength (Griffin, M. et. al. 2010). Given that we are including the SPIRE 250 and $350 \mu\text{m}$ measurements in our fitting, the $500 \mu\text{m}$ flux calibration error would have to be relative to the other two SPIRE bands and so is likely smaller than 15%. In addition, we would expect to see no correlation between the excess and ISM condition tracers, yet we see weak correlations (Fig. 3).

For 3), a wavelength dependent increase in the dust emissivity law at $500 \mu\text{m}$ on the order of 10% is possible (Paradis et al. 2009a). This variation may be attributed to the dust grains amorphous/crystalline nature, size distribution, temperature, and ma-

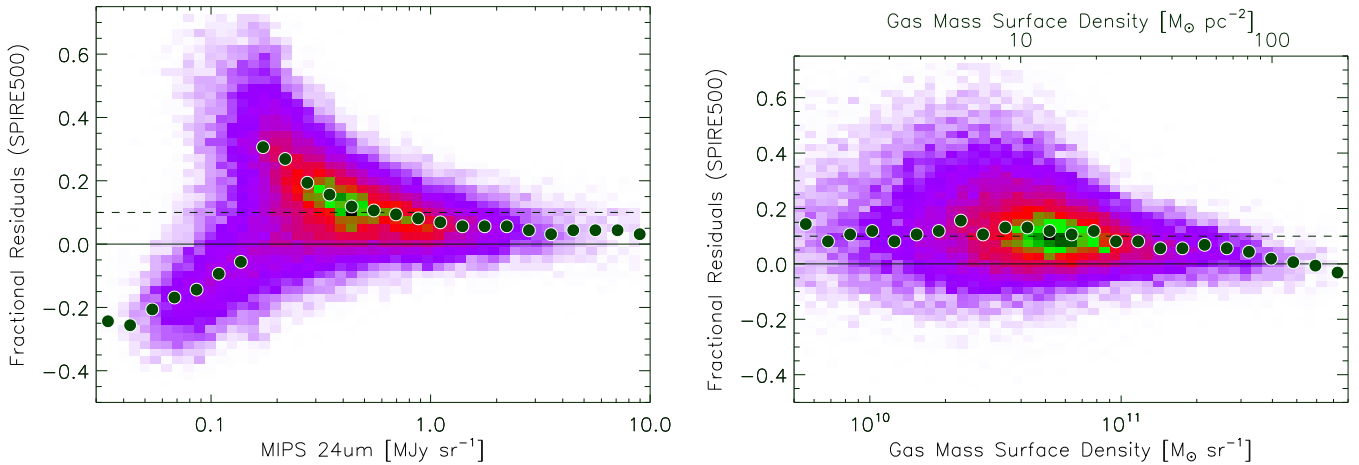


Fig. 3. The 500 μm excess is plotted versus MIPS 24 μm flux and total gas mass surface density using the 38'' resolution images. The total gas mass is derived from HI and CO observations (Kim et al. 2003; Fukui et al. 2008) assuming $X_{\text{CO}} = 7 \times 10^{20} \text{ cm}^{-2} (\text{K km s}^{-1})^{-1}$ (Fukui et al. 2008) and an overall 36% increase in the gas mass to account for the associated He gas. The density of points is coded from low to high as purple-red-green-black. The solid and dashed black lines give the zero and 10% excess values, respectively. The solid points give the values of the mode in equally spaced logarithmic bins. On average, the residuals are markedly negative at low MIPS 24 μm fluxes indicating that below these fluxes, the residuals are affected by background subtraction or fitting errors.

terial (Henning et al. 1995; Meny et al. 2007). For example, if the 500 μm excess is due to small grains having a different β than large grains, we would expect the excess to be correlated with the MIPS 24 μm emission (Reach et al. 1995). Yet the excess is weakly anti-correlated with MIPS 24 μm flux (Fig. 3).

For 4), very cold dust that only emits at $\geq 500 \mu\text{m}$ is physically possible. The very coldest dust would necessarily be the dust that is best shielded and, thus, we would then expect the excess to be strongest in the highest density regions and regions with the lowest radiation fields. Figure 3 gives a conflicting answer as we see the largest excesses in the faintest 24 μm regions (as expected) and least dense regions (not as expected).

4. Conclusions

We investigate the importance of $>200 \mu\text{m}$ data in determining dust temperatures and masses using new *Herschel* SPIRE observations of the LMC (taken for the HERITAGE Key Project as part of the *Herschel* Science Demonstration phase) combined with existing IRAS 100 μm and *Spitzer* MIPS 160 μm images. We fit the observations with a model consisting of dust emitting as a single temperature blackbody modified with an emissivity law proportional to $\lambda^{-\beta}$. For fixed values of β , fits using only the 100–160 μm data give dust temperatures and masses that are on average up to 8% and 23% different from fits using the same β and the 100–350 μm data. The new SPIRE observations allowed us to determine that $\beta = 1.5$ minimizes the residuals from 100 to 350 μm . Using a $\beta = 2.0$ for the 100–160 μm and a $\beta = 1.5$ for the 100–350 μm fits results in an increase of 10% for the dust temperature and a decrease in the dust mass by 36%.

On average, there is a fractional excess at 500 μm of $\sim 10\%$. The origin of the fractional excess is unlikely to be due to our fitting algorithm or a flux calibration error, but it could be due to either very cold dust that emits only $\geq 500 \mu\text{m}$ or a variation in the wavelength dependent change in the dust emissivity. Planned HERITAGE observations of the LMC and SMC will allow for a more detailed investigation of including $> 200 \mu\text{m}$ data (mainly

the 500 μm excess) due to better quality PACS and SPIRE images (optimized observations and cross-scans).

Acknowledgements. We acknowledge financial support from the NASA *Herschel* Science Center, JPL contracts # 1381522 & 1381650. M.R. is supported by FONDECYT No1080335 and FONDAP No15010003. We thank the contributions and support from the European Space Agency (ESA), the PACS and SPIRE teams, the *Herschel* Science Center and the NASA *Herschel* Science Center (esp. A. Barbar and K. Xu) and the PACS and SPIRE data center at CEA-Saclay, without which none of this work would be possible. We thank the referee, Thomas Henning, for suggestions that improved the clarity of this paper.

References

- Agladze, N. I., Sievers, A. J., Jones, S. A., Burlitch, J. M., & Beckwith, S. V. W. 1996, *ApJ*, 462, 1026
- Bernard, J.-P., Reach, W. T., Paradis, D., et al. 2008, *AJ*, 136, 919
- Dale, D. A., Bendo, G. J., Engelbracht, C. W., et al. 2005, *ApJ*, 633, 857
- Draine, B. T., Dale, D. A., Bendo, G., et al. 2007, *ApJ*, 663, 866
- Dunne, L., Eales, S., Edmunds, M., et al. 2000, *MNRAS*, 315, 115
- Finkbeiner, D. P., Davis, M., & Schlegel, D. J. 1999, *ApJ*, 524, 867
- Fukui, Y., Kawamura, A., Minamidani, T., et al. 2008, *ApJS*, 178, 56
- Galametz, M., Madden, S., Galliano, F., et al. 2009, *A&A*, 508, 645
- Galliano, F., Dwek, E., & Charnial, P. 2008, *ApJ*, 672, 214
- Galliano, F., Madden, S. C., Jones, A. P., Wilson, C. D., & Bernard, J.-P. 2005, *A&A*, 434, 867
- Gordon, K. D., Clayton, G. C., Misselt, K. A., Landolt, A. U., & Wolff, M. J. 2003, *ApJ*, 594, 279
- Gordon, K. D., Engelbracht, C. W., Rieke, G. H., et al. 2008, *ApJ*, 682, 336
- Griffin, M. et al. 2010, *A&A*, this issue
- Henning, T., Michel, B., & Stognienko, R. 1995, *Planet. Space Sci.*, 43, 1333
- Hilditch, R. W., Howarth, I. D., & Harries, T. J. 2005, *MNRAS*, 357, 304
- Kim, S., Staveley-Smith, L., Dopita, M. A., et al. 2003, *ApJS*, 148, 473
- Laor, A. & Draine, B. T. 1993, *ApJ*, 402, 441
- Meixner, M., Gordon, K. D., Indebetouw, R., et al. 2006, *AJ*, 132, 2268
- Meixner, M. et al. 2010, *A&A*, this issue
- Meny, C., Gromov, V., Boudet, N., et al. 2007, *A&A*, 468, 171
- Miville-Deschênes, M.-A. & Lagache, G. 2005, *ApJS*, 157, 302
- Paradis, D., Bernard, J., & Mény, C. 2009a, *A&A*, 506, 745
- Paradis, D., Reach, W. T., Bernard, J., et al. 2009b, *AJ*, 138, 196
- Reach, W. T., Dwek, E., Fixsen, D. J., et al. 1995, *ApJ*, 451, 188
- Roman-Duval, J. et al. 2010, *A&A*, this issue
- Russell, S. C. & Dopita, M. A. 1992, *ApJ*, 384, 508
- Schaefer, B. E. 2008, *AJ*, 135, 112
- Stansberry, J. A., Gordon, K. D., Bhattacharya, B., et al. 2007, *PASP*, 119, 1038

Staveley-Smith, L., Kim, S., Calabretta, M. R., Haynes, R. F., & Kesteven, M. J.
2003, MNRAS, 339, 87
Swinyard, B. et al. 2010, A&A, this issue
Willmer, C. N. A., Rieke, G. H., Le Floch, E., et al. 2009, AJ, 138, 146

- ¹ Space Telescope Science Institute, 3700 San Martin Drive, Baltimore, MD 21218, USA e-mail: kgordon@stsci.edu
- ² CEA, Laboratoire AIM, Irfu/SAP, Orme des Merisiers, F-91191 Gif-sur-Yvette, France
- ³ Centre d' Étude Spatiale des Rayonnements, CNRS, 9 av. du Colonel Roche, BP 4346, 31028 Toulouse, France
- ⁴ Department of Astronomy, University of Maryland. College Park, MD 20742, USA
- ⁵ Observatoire Astronomique de Strasbourg, 11, rue de l'universite, 67000 STRASBOURG, France
- ⁶ Steward Observatory, University of Arizona, 933 North Cherry Ave., Tucson, AZ 85721, USA
- ⁷ Centre for Supercomputing and Astrophysics, Swinburne University of Technology, Hawthorn VIC 3122, Australia
- ⁸ CSIRO Australia Telescope National Facility, PO Box 76, Epping NSW 1710, Australia
- ⁹ Sterrewacht Leiden, Leiden University, P.O. Box 9513, NL-2300 RA Leiden, The Netherlands
- ¹⁰ Jodrell Bank Centre for Astrophysics, Alan Turing Building, School of Physics & Astronomy, University of Manchester, Oxford Road, Manchester M13 9PL, United Kingdom
- ¹¹ Astronomy & Space Science, Sejong University, 143-747, Seoul, South Korea
- ¹² 314 Physics Building, Department of Physics and Astronomy, University of Missouri, Columbia, MO 65211, USA
- ¹³ Department of Physics and Astronomy, University College London, Gower Street, London WC1E 6BT, UK
- ¹⁴ MSSL, University College London, Holmbury St. Mary, Dorking, Surrey RH5 6NT, U.K.
- ¹⁵ Visiting Scientist at Smithsonian Astrophysical Observatory, Harvard-CfA, 60 Garden St., Cambridge, MA, 02138, USA
- ¹⁶ Departamento de Astronomia, Universidad de Chile, Casilla 36-D, Santiago, CHILE
- ¹⁷ Spitzer Science Center, California Institute of Technology, MS 220-6, Pasadena, CA 91125, USA
- ¹⁸ Stratospheric Observatory for Infrared Astronomy, Universities Space Research Association, Mail Stop 211-3, Moffett Field, CA 94035